IEEE Transactions on Nuclear Science, Vol. NS-28, No. 3, June 1981

A MATHEMATICAL MODEL FOR POSITRON-EMISSION TOMOGRAPHY SYSTEMS HAVING TIME-OF-FLIGHT MEASUREMENTS

Donald L. Snyder, Lewis J. Thomas, Jr., and Michel M. Ter-Pogossian
Department of Electrical Engineering
Biomedical Computer Laboratory,
and
Mallinckrodt Institute of Radiology
Washington University
St. Louis, Missouri 63110

Abstract

Improvements in high speed electronics and scintillation-crystal technology now permit usable differential time-of-flight measurements to be made in tomography systems that employ coincidence detection of the annihilation photons created with positron emitting radionuclides. A mathematical model for these new measurements is developed in this paper. Reconstruction algorithms and their signal-to-noise ratio performance are given.

I. Introduction

Tomography systems that employ positron-annihilation coincidence detection have been under intensive development for the past few years for use in medical diagnosis and physiological studies [1]. In these systems, a quantity of a radioactively labeled substance is introduced into a region of interest in a patient. Substances such as carbon-11 labeled palmitate, carbon-11 labeled hemoglobin, carbon-11 labeled glucose, nitrogen-13 labeled ammonia, and oxygen-15 labeled water are used because their distributions in tissue are governed by metabolic or physico-chemical processes of interest. Moreover, and importantly for the systems being developed, the radioactive mechanisms in the labels of these substances produce positrons, each of which, in turn, interacts with an electron in an annihilation that creates two 511 keV photons. These photons propagate in opposite directions and can be sensed with scintillation detectors placed in an array surrounding the patient, as shown in Fig. 1. In this way, photon detections occurring within a small time interval in two opposing scintillation detectors define a cylindrical volume in which an annihilation has occurred. The quantitative characteristics of this volume are determined by the shape and geometry of the detectors and the shape and geometry of lead collimators designed to reduce random coincidences [2]. Coincidence pairs collected over the entire time course of a diagnostic procedure can be processed using what are now standard algorithms of computed tomography to produce cross sections of radioactivity distributions that are useful, with other medical information, for clinical diagnosis of abnormalities of the heart, brain, and other organs of the body [3].

Besides propagating in opposite directions, there is another property that annihilation photons have, a property heretofore unused in emission tomography systems. The two photons are created simultaneously at the location where the annihilation occurs. This location then determines the differential time of flight of the two annihilation photons to the two opposing detectors which sense them. However, because of the physical size and chemical composition of crystals used in scintillation detectors, the properties of photomultipliers, and the limitations of coincidence detection circuitry, it has not been feasible in the past to measure, with a useful accuracy, the time difference between the arrivals of the two photons at the opposing detectors. Since photons propagate at the speed of light, a 10 cm spatial resolution requires that a 2/3 ns time differential be measured, and this has been a difficult performance goal to achieve. Recent trends in both detector and electronic technology, however, are toward permitting more accurate differential time of flight measurements to be made. At the extreme, yet to be realized, where such measurements could be made with arbitrary accuracy, spatial distributions of radioactivity could be estimated simply by histograms derived with no more than a scaling to account for the propagation velocity of photons, and none of the time-consuming, hardware-expensive calculations required to implement a tomography reconstruction algorithm would be required. However, at the present time and in at least the near future, the uncertainty associated with time of flight measurements is still so great that this simple histogram approach is inadequate for producing clinically significant reconstructions of radioactivity, and more sophisticated processing is needed. Therefore, we are motivated to propose a model for differential time of flight measurements, derive reconstruction algorithms based on our model, and predict the signal-to-noise ratio performance of these algorithms.

The concept of utilizing time of flight information for estimating the concentration of a positron-emitting radionuclide is not new. In a survey of radioisotope cameras in 1966, Anger [4] mentioned the possibility but concluded that then available sodium iodide scintillation detectors were too slow to make the approach practical. Burnham, Aronow, and Brownell [5] discussed this methodology at a symposium on the localization of tumors, and they noted the need for a fast, high density scintillator to be developed. In 1968, Brownell and his co-workers [6] described the design of an experimental system utilizing plastic scintillators to measure propagation time with a resolution of about 400 ps. Nickles and Meyers [7] proposed in 1977 the design of a positron camera for nuclear medicine in which photon propagation times are used for the three-dimensional positioning of an annihilation event. Also in 1977 in a discussion of the need for new developments in nuclear medicine, Budinger [8] noted that the performance of a positron ring detector system could be improved by incorporating time of flight information, and he estimated that with the ability of achieving a positional uncertainty of 3 cm or less along the line of flight, there would be an improvement in the signal-to-noise ratio by as much as a factor of 10. In 1979, a research group at the Laboratoire d'Electronique et de Technologie de l'Informatique in Grenoble, France [9,10] presented the advantages of incorporating time of flight information into positron emission tomography. This has motivated our group to initiate the development of a new emission tomography system that uses time of flight data [11].

Manuscript received by IEEE, December 23, 1981.

This work was supported by the National Institutes of Health under Grants RR00396 (from the Division of Research Resources), HL 13851, and HL 25944 and by the National Science Foundation under Grant ENG76-11565.

0018-9499/81/0600-3575$00.75© 1981 IEEE

II. Model Development

To introduce our model, we briefly describe the process by which the differential time of flight for two photons is measured, thereby determining the location of the positron annihilation that created them. When a 511 keV photon is absorbed by the crystal in a scintillation detector, its energy is converted into optical energy, a brief flash of light, which is detected by an adjacent photomultiplier. A threshold circuit discriminates the detected event in the current from the photomultiplier and triggers a circuit which initiates a positive going ramp voltage. This ramp is terminated by a similar circuit which responds to the detection of the arrival of the second 511 keV photon in the opposing crystal. The voltage level achieved by the ramp is proportional to the differential time of flight and contains the information about where the annihilation event occurred along the line connecting the two detectors involved.

Several factors influence the accuracy with which the time of occurrence of photon absorptions can be determined. These include the physical extent of the crystal needed to insure that photons are absorbed with high probability, the chemical composition of the crystal material, pulse spreading due to transit time effects in the photomultiplier, and the sensitivity of the triggering circuitry that initiates and terminates the ramp voltage. The cumulative effect of these various factors is a positional uncertainty. Fig. 2 shows a distribution of this uncertainty recently measured in our laboratory. This uncertainty is somewhat less than that reported previously in [11]. At least into the near future, it appears that the standard deviation of positional errors will remain in excess of about 2.5 cm (6 cm full width at half maximum (FWHM)), which is too large for these measurements to be useful along without further signal processing. In our later considerations, we approximate the distribution of errors for positions derived from time of flight data by a zero mean normal distribution with variance σ_e^2. The range of σ_e^2 of practical interest is 0.42 to 4.2 cm (1.0 to 10.0 cm FWHM).

Shown in Fig. 3 (from [2]) are data obtained experimentally from a point source of radioactivity placed between two detectors. The measured activity is seen to be a very slowly changing function of the location of the source along the line connecting the detectors and a rapidly decreasing function, with about a 1 cm FWHM distribution, of the source position transverse to this line. In our later considerations, we approximate this distribution in the transverse direction by a zero-mean normal distribution with variance σ_b^2. The range of σ_b^2 of practical interest is 0.2 to 0.6 cm (0.5 to 1.5 cm FWHM). The small variation as the source is moved along the connecting line will be ignored.

Measurement Point Process

We now define a random point process which we call the "measurement point process." This process plays a central role in designing and evaluating reconstruction algorithms using time-of-flight measurements. With reference to Fig. 4, consider a continuous detector ring surrounding the region containing radioactivity. A measurement associated with a single annihilation identifies the two locations on the ring where the annihilation photons are detected and the differential time of arrival Δt of the photons at these locations. This measurement then defines the line ℓ indicated in Fig. 4 and a point u along the line. The line, and therefore the measurement, can be parameterized by (u,θ), where θ is the angle of line as shown. In other words, an individual measurement determines a point (u,θ) in a three-dimensional measurement space $M = R^2 \times [0,\pi]$, where R^2 denotes two-dimensional Euclidean space. The measurements obtained over an entire experiment then form a point process on M. Denote by $N(A \times \Theta)$ the counting process associated with this measurement point process, where $N(A \times \Theta)$ is the number of measurement points having positions u in the set A of R^2 and angles θ in the set Θ of $[0,\pi]$.

The statistical properties of the measurement point process are determined by the measurement system and by another underlying and unobservable point process we call the "annihilation point process." Points of this latter process just identify the location in R^2 of each annihilation. From physical considerations [12, page 746], this annihilation point process is well modeled mathematically as a Poisson process on R^2 with a spatially dependent intensity function that is proportional to the concentration of radioactivity. We let $\lambda(x)$ denote the intensity of the annihilation point process at the location x in R^2. One important property implied by the Poisson nature of the annihilation point process is that given the number of annihilations in an experiment, their locations are the same as if selected independently and identically according to the probability density $\Lambda^{-1}\,\lambda(x)$, where [13, page 65]

$$\Lambda = \iint_{R^2} \lambda(x)\,dx.$$

Also, the total number of annihilations has a Poisson distribution with parameter Λ, so Λ is the total average number of annihilations.

Fig. 5 defines the relationship between the annihilation and measurement point processes. An annihilation occurring at x is measured as the point (u,θ), where $u = x + \varepsilon(\theta)$. Here, $\varepsilon(\theta)$ is a two-dimensional measurement-error vector with a component ε_e parallel to the center line of the detector pair and a component ε_b transverse to this line. We assume that the measurement error ε associated with an annihilation at x is independent of x as well as the locations and measurement errors of all other annihilations. The conditional probability density function of $\varepsilon(\theta)$ for θ given will be denoted by $p(\varepsilon|\theta)$, where for later calculations we employ the two-dimensional normal density

$$p(\varepsilon|\theta) = [2\pi \det^{\frac{1}{2}}(R(\theta))]^{-1} \exp\{-\tfrac{1}{2}\varepsilon' R^{-1}(\varepsilon)\}, \tag{1}$$

with the covariance matrix $R(\theta)$ given by

$$R(\theta) = T(\theta)\begin{bmatrix} \sigma_e^2 & 0 \\ 0 & \sigma_b^2 \end{bmatrix} T'(\theta), \tag{2}$$

where the prime "'" denotes matrix transpose, σ_e^2 and σ_b^2 are error variances along and transverse to the detector center line, respectively, and $T(\theta)$ is the rotation matrix

$$T(\theta) = \begin{bmatrix} \cos\theta & \sin\theta \\ -\sin\theta & \cos\theta \end{bmatrix}$$

The determinant of $R(\theta)$ needed in (1) is $\det(R(\theta)) = \sigma_e^2\sigma_b^2$.

We also assume that annihilation photons propagate isotropically, independent of the location x where they are created; in other words, the probability density of θ is $1/\pi$ for $0 \le \theta \le \pi$ regardless of x.

It now follows from these assumptions that the measurement point process is a Poisson point process with an intensity function that is the two-dimensional convolution of the intensity $\lambda(x)$ of the annihilation point process and the error density $p(x|\theta)/\pi$; that is, if $\mu(u,\theta)$ denotes the intensity of the measurement point process, then

$$\mu(u,\theta) = (1/\pi)\iint_{R^2} p(u-x|\theta)\lambda(x)dx. \tag{3}$$

This can be seen as follows. Given the total number, say n, of annihilations, each measurement point u is the sum of two independent random variables, x and $\varepsilon(\theta)$, which with the uniform distribution for θ, implies (3). Also, the locations of the measurement points are independent because those of the annihilation point process are and because measurement errors are independent. Finally, since n is Poisson distributed and is also the total number of measurement points, we conclude [13, page 117] that the measurement point process is a Poisson process on $R^2\times[0,\pi]$ with the intensity function $\mu(u,\theta)$ given in (3).

Preimage Array

By a "preimage array" we mean a memory array wherein measured data are collected and saved, usually in real time as an experiment is conducted. Data in the preimage array are subsequently processed using an appropriate algorithm in order to reconstruct the distribution of radioactivity. In our model, data in the preimage array are derived from the output of a linear filter having the measurement point process as its input. A variety of preimage arrays of potential interest are included by appropriately selecting the weighting function of the linear filter. We shall give examples of two- and three-dimensional arrays. First, we consider a three-dimensional preimage defined by samples of the function $f(z,\theta)$ defined by

$$f(z,\theta) = \int_0^\pi\iint_{R^2} w(z-u|\theta)I_{\delta_\theta}(\theta-\phi)N(du\times d\phi), \tag{4}$$

where

$$I_{\delta_\theta}(\theta) = 1, \quad -\delta_\theta/2 \le \theta \le \delta_\theta/2,$$

and

$$I_{\delta_\theta}(\theta) = 0, \text{ otherwise},$$

and where $w(z|\theta)$ is a weighting function selected by the designer to achieve a desired three-dimensional preimage array. The integral in (4) is interpreted as

$$f(z,\theta) = \begin{cases} 0, & n = 0 \\ \sum_{i=1}^{n} w(z-u_i|\theta)I_{\delta_\theta}(\theta-\phi_i), & n \ge 1 \end{cases} \tag{5}$$

where n is the total number of measurement points and the ith point is located at (u_i,ϕ_i). Thus, to get $f(z,\theta)$, we shift the weighting function to the spatial coordinate u of each measurement point and then sum these responses for all points having their angle coordinate with $\delta_\theta/2$ of θ.

We now give several examples of two- and three-dimensional preimage arrays of potential interest.

Example 1. Suppose in (4) that

$$w(z|\theta) = I_\delta(z), \tag{6}$$

where

$$I_\delta(z) = 1, \quad -\delta/2 \le z_1 \le \delta/2, \ -\delta/2 \le z_2 \le \delta/2$$

and

$$I_\delta(z) = 0, \quad \text{otherwise}.$$

Then,

$$f(z,\theta) = \int_0^\pi\iint_{R^2} I_\delta(z-u)I_{\delta_\theta}(\theta-\phi)N(du\times d\phi) \tag{7}$$

is the number of measurement points in a three-dimensional, rectangular resolution-cell centered at (z,θ) in $R^2\times[0,\pi]$ and having volume $\delta^2\delta_\theta$. We note for later use that for this choice of w, that $f(z,\theta)$ is Poisson distributed with parameter

$$\alpha(z,\theta) = \int_0^\pi\iint_{R^2} I_\delta(z-u)I_{\delta_\theta}(\theta-\phi)\mu(u,\phi)du d\phi, \tag{8}$$

where μ is given in (3). Thus, for δ and δ_θ sufficiently small,

$$\alpha(z,\theta) = \delta^2\delta_\theta(1/\pi)\iint_{R^2} p(u-x|\theta)\lambda(x)dx. \tag{9}$$

Example 2. Because of the circular symmetry that results, we find it convenient for later numerical comparisons of preimage arrays to consider also a circular resolution cell $c_\delta(z)$ defined by

$$c_\delta(z) = 1, \quad |z| \le \delta/2 \quad \text{and} \quad c_\delta(z) = 0, \text{ otherwise}. \tag{10}$$

If $w(z|\theta) = c_\delta(z)$ in (4), then $f(z,\theta)$ is the number of measurement points in the cylinder $c_\delta(z-u)\ I_{\delta_\theta}(\theta-\phi)$ centered at (z,θ).

Example 3 ("projection" array). Suppose $w(z|\theta)$ is unity for z within the strip of width δ at angle θ shown in Fig. 6 and that $w(z|\theta)$ is zero otherwise. Then, $f(z,\theta)$ is a unity-weighted, strip integration at angle θ [14]. We call the array that results by sampling this $f(z,\theta)$ in the obvious way the "projection array." This is the array assumed for conventional, positron-emission tomography-systems.

The following examples result in two-dimensional preimage arrays of potential interest when time-of-flight data are available, including all two-dimensional arrays so far proposed when time of flight data are available. These are derived from samples of the two-dimensional filtering of the measurement point process defined by

$$f(z) = \lim_{\delta_\theta \to 0} (1/\delta_\theta) \int_0^\pi f(z,\theta)d\theta$$

$$= \int_0^\pi \iint_{R^2} w(z-u|\phi)N(du\times d\phi). \qquad (11)$$

Example 4 ("unfiltered back projection" array). If $w(z|\theta)$ in (11) is selected as in Ex. 3, the result is the unfiltered back-projection array of conventional positron-emission tomography. A known two-dimensional filtering of this array results in an estimate of the radioactivity distribution that does not use the time-of-flight information.

Example 5 ("most likely position" array). If $w(z|\theta)$ in (11) is selected as in Ex. 1, the resulting $f(z)$ is the number of measurement points in $I_\delta(z-u)$ regardless of their measured angles. We call the preimage array that results by sampling this $f(z)$ on the obvious lattice in R^2 the "most likely position" array because it corresponds to the intuitively appealing approach of incrementing by unity the resolution cell in which the position u of the measurement point (u,θ) falls. Note that the measured position u is the maximum likelihood estimate of the annihilation position x for the two-dimensional normal distribution of measurement errors in (1).

Example 6 ("confidence weighted" array). Suppose that the model in (1) holds and in (11) that

$$w(z|\theta) = [2\pi \det^{\frac{1}{2}}(R(\theta))]^{-1} \exp[-\tfrac{1}{2} z' R^{-1}(\theta) z],$$

where $R(\theta)$ is the covariance matrix in (2). The resulting $f(z)$ is the normally weighted, unfiltered back-projection considered by the L.E.T.I. group [9,10]. We term the preimage array that results by sampling $f(z)$ the "confidence weighted" array because, in contrast to Ex. 5 where unit weight is placed in the single most likely resolution cell for each measurement point, every cell is weighted in proportion to the posterior probability that the annihilation point occurred in that cell given the measurement point (u,θ).

Data in the preimage array are to be processed using an appropriate algorithm to produce an estimate of a desired image of the distribution of radioactivity. We denote the desired image by $d(x)$ and assume that this is related to the intensity $\lambda(x)$ of the annihilation point process according to the convolution

$$d(x) = \iint_{R^2} h(x-x')\lambda(x')dx', \qquad (12)$$

for some specified weighting function $h(x)$. Choices of h that are of interest include: $h(x) = \delta(x)$, $h(x) = I_\delta(x)$, and $h(x) = c_\delta(x)$, where $\delta(x)$ is a two-dimensional impulse, and $I_\delta(x)$ and $c_\delta(x)$ are as defined in (6) and (10), respectively. For the first choice, $d(x) = \lambda(x)$, and for the other two, $d(x)$ is the total average number of annihilations in a square or circular resolution cell of size δ. The latter choices are of interest when it is desired to generate displays of total activity in an array of square or circular pixels, in which case an estimate of $d(x)$ is sampled on the obvious lattice and displayed as a constant over the corresponding pixel. Because of the circular symmetry that results, we will later use $h(x) = c_\delta(x)$ for numerical comparisons.

We next address the issue of estimating $d(x)$ given the data collected in the preimage array. In identifying the general form of the estimation algorithms, we suppress the sampling issues by considering the two- and three-dimensional functions $f(z)$ and $f(z,\theta)$ from which the preimage arrays are obtained.

III. Reconstruction Algorithms

The maximum likelihood estimate $\hat{\alpha}(z,\theta)$ of the mean parameter $\alpha(z,\theta)$ in Ex. 1, given the counts $f(z,\theta)$, is simply $f(z,\theta)$ because the measurement point process is a Poisson process. Thus, for δ and δ_θ sufficiently small, and for a fixed value of

$$\hat{\alpha}(z,\theta) = \int_0^\pi \iint_{R^2} I_\delta(z-u) I_{\delta_\theta}(\theta-\phi)N(du\times d\phi)$$

$$\approx \delta^2 \delta_\theta (1/\pi) \iint_{R^2} p(z-x|\theta)\hat{\lambda}(x)dx.$$

Multiplying by $(\delta^2\delta_\theta)^{-1} w(v-z|\theta)$, integrating with respect to z, and letting δ tend to zero, we obtain

$$(1/\pi)\iint_{R^2} g(v-x|\theta)\hat{\lambda}(x)dx = \delta_\theta^{-1} f(v,\theta), \qquad (13)$$

where $g(x|\theta)$ is defined by the convolution

$$g(x|\theta) = \iint_{R^2} p(x-x'|\theta)w(x'|\theta)dx'.$$

Since $d(x)$ and $\lambda(x)$ are related by the convolution in (12), we have from (13) that the estimate of $d(x)$ is the solution to the following integral equation

$$(1/\pi)\iint_{R^2} g(v-x|\theta)\hat{d}(x)dx = \delta_\theta^{-1} \iint_{R^2} h(v-x)f(x,\theta)dx. \qquad (14)$$

Algorithms for two-dimensional preimage arrays are obtained from this expression by integrating both sides with respect to θ, letting δ_θ tend to zero, and using (11). The result is

$$\iint_{R^2} \bar{g}(v-x)\hat{d}(x)dx = \iint_{R^2} h(v-x)f(x)dx, \qquad (15)$$

where

$$\bar{g}(x) = (1/\pi)\int_0^\pi g(x|\theta)d\theta. \qquad (16)$$

Equation (15) can be solved for $\hat{d}(x)$ in the frequency domain as follows. Define the two-dimensional Fourier transform $A(\xi)$ of any function $a(x)$ by

$$A(\xi) = \iint_{R^2} a(x)\exp[-j2\pi\xi' x]dx.$$

Transforming (15) yields

$$\hat{D}(\xi) = \overline{G}^{-1}(\xi)H(\xi)F(\xi), \tag{17}$$

which defines the image array in terms of a two-dimensional preimage.

Example 7. Suppose $p(\varepsilon|\theta)$ is the two-dimensional density in (1) and $w(z|\theta)$ is selected for the confidence weighted preimage array of Ex. 6. We then find that

$$\overline{G}(\xi) = \exp[-2\pi^2(\sigma_e^2+\sigma_b^2)|\xi|^2]\; I_0[2\pi^2(\sigma_e^2-\sigma_b^2)|\xi|^2] \tag{18}$$

where $I_0(\cdot)$ is the zero-order Bessel function of the second kind. In implementing (17) to create the image $\hat{d}(x)$, $\overline{G}^{-1}(\xi)H(\xi)$ would be set to zero for $|\xi|$ greater than a value selected in accordance with the desired sampling resolution and some form of window function might be included. By virtue of the asymptotic properties of the Bessel function, $\overline{G}^{-1}(\xi)$ becomes proportional to $|\xi|$ for $\sigma_b^2 = 0$ and σ_e^2 large. Consequently, (17) shows how to generalize the ramp filter of conventional positron-emission tomography when time-of-flight measurements are available.

In this section we have indicated how reconstruction algorithms for two-dimensional preimage arrays follow from (14). In a later publication, we will pursue this matter further and present results of computer implementations of specific algorithms. We now give expressions for the signal-to-noise ratio performance of reconstruction algorithms.

IV. Performance Evaluation

Preimage arrays, $f(x,\theta)$ or $f(x)$, and the desired image, $d(x)$, are specified by selecting the weighting functions $w(x|\theta)$ and $h(x)$, respectively. For each selection, there is a corresponding algorithm to create the image array, $\hat{d}(x)$. It is important to be able to evaluate the performance of algorithms so that various selections can be compared quantitatively. Such evaluations and comparisons are given in this section. The aspects of our model used to accomplish this are that the image, $\hat{d}(x)$, is a linear filtering of the measurement point process and the measurement point process is a Poisson process having an intensity with a known relation to the intensity of the annihilation point process and the measurement errors.

Bias

The "bias" $b(x)$ in reconstructing $d(x)$ is defined by

$$b(x) = E[\hat{d}(x) - d(x)], \tag{19}$$

where $E(\cdot)$ denotes the expectation or average. We evaluate the bias for two-dimensional preimage arrays by examining the transform $B(\xi)$ of $b(x)$. The image $\hat{d}(x)$ is termed "unbiased" if $b(x) = 0$.

From (12) and (17), we have for a two-dimensional preimage array that there holds

$$B(\xi) = \overline{G}^{-1}(\xi)H(\xi)E[F(\xi)] - H(\xi)\Lambda(\xi). \tag{20}$$

Since the measurement point process is a Poisson process, it follows from (11) that [13, page 171]

$$E[F(\xi)] = (1/\pi)\int_0^\pi W(\xi|\theta)P(\xi|\theta)\Lambda(\xi)d\theta = \overline{G}(\xi)\Lambda(\xi). \tag{21}$$

Substitution into (20) then shows that $\hat{d}(x)$ is unbiased for any desired image and two-dimensional preimage array of the type included in our model.

Error Covariance

The covariance of the error $\hat{d}(x) - d(x)$ is defined by

$$K(x_1,x_2) = E\{[\hat{d}(x_1) - d(x_1)][\hat{d}(x_2) - d(x_2)]\}. \tag{22}$$

This can be evaluated for two-dimensional preimage arrays as follows. Define $\Gamma(\xi|\phi)$ by

$$\Gamma(\xi|\phi) = \overline{G}^{-1}(\xi)H(\xi)W(\xi|\phi), \tag{23}$$

and let $\gamma(x|\phi)$ be the inverse two-dimensional transform of this function,

$$\gamma(x|\phi) = \iint_{R^2} \Gamma(\xi|\phi)\exp[j2\pi\xi'x]d\xi.$$

Then, from (11) and (17),

$$\hat{d}(x) = \int_0^\pi\iint_{R^2} \gamma(x-u|\phi)N(du\times d\phi). \tag{24}$$

Since the measurement point process is a Poisson process, it follows that [13, page 172]

$$K(x_1,x_2) = (1/\pi)\int_0^\pi K(x_1,x_2|\phi)d\phi, \tag{25}$$

where we define

$$K(x_1,x_2|\phi) = \pi\iint_{R^2} \gamma(x_1-u|\phi)\gamma^*(x_2-u|\phi)\mu(u,\phi)du, \tag{26}$$

where the "*" denotes complex conjugation. Using (24) and defining

$$M(\xi|\phi) = \iint_{R^2} \mu(u,\phi)\exp[-j2\pi\xi'u]du,$$

we express $K(x_1,x_2|\phi)$ alternatively as

$$K(x_1,x_2|\phi) = \pi\iint_{R^2}\iint_{R^2} \Gamma(\xi_1|\phi)\Gamma^*(-\xi_2|\phi)M(\xi_1-\xi_2|\phi) \times \exp\{j2\pi[\xi_1'x_1-\xi_2'x_2]\}d\xi_1 d\xi_2. \tag{27}$$

When we substitute (24) into this expression and use

$$M(\xi|\phi) = (1/\pi)P(\xi|\phi)\Lambda(\xi),$$

which follows from (3), we conclude that

$$K(x_1,x_2) = \iint_{R^2}\iint_{R^2} A(\xi_1)A^*(-\xi_2)B(\xi_1,\xi_2)\Lambda(\xi_1-\xi_2) \times \exp\{j2\pi[\xi_1'x_1-\xi_2'x_2]\}d\xi_1 d\xi_2, \tag{28}$$

where A and B are defined by

$$A(\xi) = \overline{G}^{-1}(\xi)H(\xi) = [(1/\pi)\int_0^\pi P(\xi|\phi)W(\xi|\phi)d\phi]^{-1}H(\xi)$$

and

$$B(\xi_1,\xi_2) = (1/\pi)\int_0^\pi W(\xi_1|\phi)W^*(-\xi_2|\phi)P(\xi_1-\xi_2|\phi)d\phi.$$

Since this integral expression depends on W, H, P, and Λ, the error covariance for a two-dimensional preimage depends on how the preimage (W) and desired image (H) are selected, the time of flight measurement error (P), and the intensity of the annihilation point process (Λ).

Example 8 ("confidence weighted" array). For the error density in (1) and the confidence weighted preimage array in Ex. 6, we find that

$$A(\xi) = H(\xi)\exp\{2\pi^2(\sigma_e^2+\sigma_b^2)|\xi|^2\} \times I_0^{-1}[2\pi^2(\sigma_e^2-\sigma_b^2)|\xi|^2]$$

and

$$B(\xi_1,\xi_2) = \exp\{-2\pi^2(\sigma_e^2+\sigma_b^2)[|\xi_1|^2+|\xi_2|^2-\xi_1'\xi_2] \times I_0[2\pi^2(\sigma_e^2-\sigma_b^2)\beta],$$

where

$$\beta^2 = |\xi_1|^4+|\xi_2|^4-|\xi_1|^2|\xi_2|^2+4(\xi_1'\xi_2)^2 -2[|\xi_1|^2+|\xi_2|^2+|\xi_2|^2]\xi_1'\xi_2.$$

Example 9 ("most likely position" array). For the error density in (1) and the most likely position preimage array in Ex. 2, we find that

$$A(\xi) = H(\xi)W^{-1}(\xi)D(\xi)$$

and

$$B(\xi_1,\xi_2) = W(\xi_1)W^*(-\xi_2)D(\xi_1-\xi_2),$$

where

$$D(\xi) = \exp\{4\pi^2(\sigma_e^2+\sigma_b^2)|\xi|^2\}I_0[4\pi^2(\sigma_e^2-\sigma_b^2)|\xi|^2],$$

and where $W(\xi) = W(\xi|\phi)$ is the transform of the weighting function used to create the most likely position array. It is evident from (28) that whenever $W(\xi|\phi)$ is not a function of ϕ, as in this example, then $W(\xi|\phi)$ does not influence the error covariance. We find below that serious performance degradation can result from such a choice.

The general performance expressions developed in this section evidently cannot be simplified further for interesting selections of preimages and desired images. Nevertheless, they can be evaluated numerically for system comparisons. This is illustrated in the next section.

V. Performance Comparison Example

We have numerically evaluated the performance expressions of the last section under the following conditions:

a. Radioactivity is uniformly distributed over a circular region of radius R cm, with R=15, and such that a total of 10^6 annihilations occur on the average. Thus, $\lambda(x) = 10^6 c_{30}(x)$.

b. The desired image is defined by (12) with $h(x) = c_\Delta(x)$, with Δ=2 cm. Thus, $d(x) = 10^6/225$ is the average number of annihilations in a circular resolution cell of radius 1 cm.

c. The measurement error distribution is that given in (1) with $\sigma_b^2 = 0$. Thus, the only error arises in the measurement of differential time of flight.

Shown in Fig. 7 is the signal to noise ratio SNR for several preimage arrays as a function of the full width at half maximum FWHM time of flight uncertainty ($2.35\sigma_e$), where in decibels the definition of signal to noise ratio we use is

$$\mathrm{SNR} = 10\log_{10}[d^2(0)/K(0,0)] \tag{29}$$

The SNR performance is shown for the most likely position and confidence weighted preimage arrays. The graphs in Fig. 7 for these and two other situations are discussed in the following remarks.

remark 1. In the limit of arbitrarily small time of flight errors, annihilation points and measurement points coalesce, in which case measurement points falling in the resolution circle $c_\Delta(x)$ originate only from annihilation points therein. By virtue of the Poisson statistics, we expect, therefore, that $K(0,0) = d(0) = 10^6/225$. The graphs shown in Fig. 7 approach this asymptote (36.4 db) for all the preimage arrays considered.

remark 2. The limit of arbitrarily large time of flight errors corresponds to conventional emission tomography. Budinger [15, Eq. (11)] has analyzed the signal to noise ratio for this limit. All the graphs shown in Fig. 7 except that for the most likely array approach this limit asymptotically ($\Lambda(\Delta/2)^3/(1.2)^2R^3 =$ 23.1 db).

remark 3. The graphs labeled "confidence weighted" and "most likely position" in Fig. 7 indicate the performance from Ex. 8 and Ex. 9. These were obtained by computer evaluation of the performance expressions.

remark 4. Since the mechanical and electronic features of a system that collects time of flight data and one that collects conventional tomography data are nearly identical, it is of interest to consider that both types of data are collected together, in which case two images can be created. Let $\hat{d}_{TOF}(x)$ and $\hat{d}_{TOMO}(x)$ denote the two images and $K_{TOF}(x_1,x_2)$ and $K_{TOMO}(x_1,x_2)$ the corresponding error covariances. A single image that reflects the most reliable parts of each of these images is desirable. One way to define such a "pooled image" results when the estimation errors $\hat{d}_{TOF} - d$ and $\hat{d}_{TOMO} - d$ are approximated as independent and normally distributed with mean zero and variance equal to $K_{TOF}(x,x)$ and $K_{TOMO}(x,x)$, respectively. Then the maximum likelihood estimate of d(x) given $\hat{d}_{TOF}(x)$ and $\hat{d}_{TOMO}(x)$ satisfies

$$\hat{d}(x) = (1+a)^{-1}\hat{d}_{TOF}(x) + a(1+a)^{-1}\hat{d}_{TOMO}(x),$$

where $a = K_{TOF}(x,x)/K_{TOMO}(x,x)$. Furthermore, the resulting signal to noise ratio is the sum of the signal to noise ratios of the two constituent images. The graph labeled "pooled" in Fig. 7 is this performance when the TOF image is based on the "most-likely position" preimage-array.

remark 5. An heuristic argument for predicting the performance when time of flight data are available can be given using Budinger's formula [15, Eq. (11)], which predicts a signal to noise ratio equal to $0.69\, d(0)(\Delta/2R)$. The factor $(2R)^{-1}$ occurs because without time of flight information, the uncertainty in localizing an annihilation point is uniformly distributed along the image in a projection measurement. However, with time of flight data, this uncertainty is reduced to about the full width at half maximum (FWHM) time of flight uncertainty, and Budinger's formula can be modified as

$$0.69\, d(0)\Delta(\mathrm{FWHM})^{-1} = 0.69\, d(0)(\Delta/2R)(\mathrm{FWHM}/2R)^{-1},$$

so the improvement in signal to noise ratio varies inversely as the fraction FWHM/2R of the image contained within the time of flight uncertainty. This prediction would be expected to hold over the approximate range $\Delta \leq \mathrm{FWHM} \leq 2R$. The graph labeled "intuitive" in Fig. 7 is based on this argument.

VI. Conclusion

The model we have presented for time of flight measurements in positron emission tomography provides an analytical approach to developing reconstruction algorithms and predicting their performance. In comparing alternative data collection strategies in Section V, we conclude for the parameter values selected that the signal to noise ratio performance with the most likely position array is substantially inferior to that of the confidence weighted array. The pooling approach improves the performance that can be achieved with the most likely position array when conventional tomography data are also available, but the performance of the confidence weighted array is still not reached. We also observe that the intuitive approach for predicting performance provides a quick, easy way to estimate the performance for the confidence weighted array.

We note, finally, that significant performance improvement, compared to conventional emission tomography, appears to be possible for practical values of time of flight uncertainty. For instance, for the confidence weighted preimage array, we see from Fig. 7 that the gain in signal to noise ratio for FWHM=6 cm is 6.4 db or a factor of about 4.4. The implications are then that either: (1), the signal to noise ratio performance will be improved by a factor of 4.4; (2), the performance will be the same if the total radioactivity is reduced by a factor of 4.4; or (3), the performance will be the same if the data-collection time is reduced by a factor of 4.4. These gains are based on the assumption that the efficiency in detecting annihilation photons is the same with and without the time of flight measurement.

VII. References

1. M. M. Ter-Pogossian, N. A. Mullani, J. T. Hood, C. S. Higgins, and D. C. Ficke, "Design Considerations for a Positron Emission Transverse Tomograph (PETT V) for Imaging of the Brain," J. Computer Assisted Tomography, Vol. 2, pp. 539-544, 1978.

2. M. E. Phelps, E. J. Hoffman, N. A. Mullani, and M. M. Ter-Pogossian, "Application of Annihilation Coincidence Detection to Transaxial Reconstruction Tomography," J. Nucl. Med., Vol. 16, pp. 210-224, 1975.

3. M. M. Ter-Pogossian, M. S. Klein, J. Markham, R. Roberts, and B. E. Sobel, "Regional Assessment of Myocardial Metabolic Integrity In Vivo by Positron Emission Tomography with C-Labeled Palmitate," Circulation, Vol. 61, pp. 242-255, February 1980.

4. H. O. Anger, "Survey of Radioisotope Cameras," ISA Transactions, Vol. 5, pp. 311-334, 1966.

5. C. A. Burnham, S. Aronow, and G. L. Brownell, "New Instrumentation for Positron Scanning," In: Radioactive Isotopes in the Localization of Tumors (V. R. McCready et al, eds.), Grune-Stratton, New York, pp. 16-19, 1969.

6. G. L. Brownell, C. A. Burnham, S. Wilensky, S. Aronow, H. Kazemi, and D. Strieder, "New Developments in Positron Scintigraphy and the Application of Cyclotron Produced Positron Emitters," In: Medical Radioisotope Scintigraphy, Vol. 1, Proc. of a Symposium, Salzburg, August, 1968, p. 466, Vienna, IAEA, 1969.

7. R. J. Nickles and H. O. Meyer, "Design of a Three-Dimensional Positron Camera for Nuclear Medicine," Phys. Med. Biol., Vol. 23, pp. 686-695, 1978.

8. T. F. Budinger, "Instrumentation Trends in Nuclear Medicine," Seminars in Nuclear Medicine, Vol. 7, pp. 285-297, 1977.

9. R. Allemand, C. Gresset, J. Vacher, "Potential Advantages of a Cesium Flouride Scintillator for a Time of Flight Positron Camera," J. Nucl. Med., Vol. 21, pp. 153-155, 1980.

10. R. Allemand, R. Campagnolo, P. Garderet, R. Gariod, C. Gresset, C. Janin, M. Lavel, R. Odru, E. Tournier, and J. Vacher, "A New Time of Flight Method for Positron Computed Tomography," Proc. NSR/CNRS U.S./France Seminar on Biomedical Image Processing, Grenoble, May 1980.

11. N. A. Mullani, J. Markham, and M. M. Ter-Pogossian, "Feasibility of Time of Flight Positron Emission Tomography Reconstruction," J. Nucl. Med., Vol. 21, pp. 1095-1097, 1980.

12. R. D. Evans, The Atomic Nucleus, McGraw-Hill Book Co., New York, 1955.

13. D. L. Snyder, Random Point Process, John Wiley and Sons, Inc., New York, 1975.

14. R. Bracewell, "Two-Dimensional Aerial Smoothing in Radio Astronomy," Aust. J. Phys., Vol. 9, pp. 297-314, 1956.

15. T. F. Budinger, S. E. Derenzo, G. T. Gullberg, W. L. Greenberg, and R. H. Huesman, "Emission Computer Assisted Tomography with Single-Photon and Positron Annihilation Photon Emitters," J. Computer Assisted Tomography, Vol. 1, pp. 131-145, 1977.

Acknowledgement

We are pleased to acknowledge the encouragement and help of Dr. Jerome R. Cox, Jr. during the development of this work. Discussions with Ms. Nian Chang Cheng (E.E. and B.C.L.) about the pooling approach in

remark-4 and with Dr. J. Philip Miller about some of the numerical issues were helpful and appreciated.

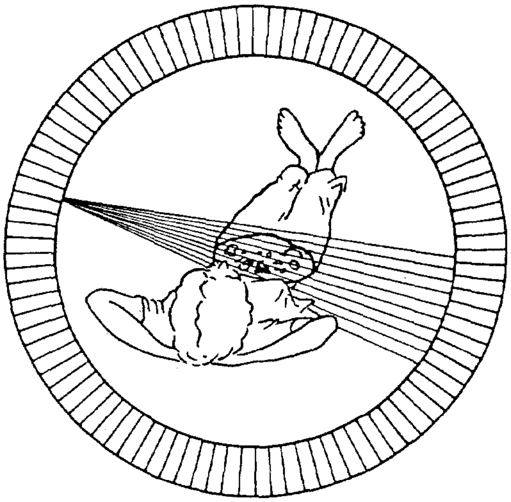

Figure 1. A Positron Emission Tomography System. Shown surrounding a patient is a circular ring of scintillation detectors used to observe annihilation photons.

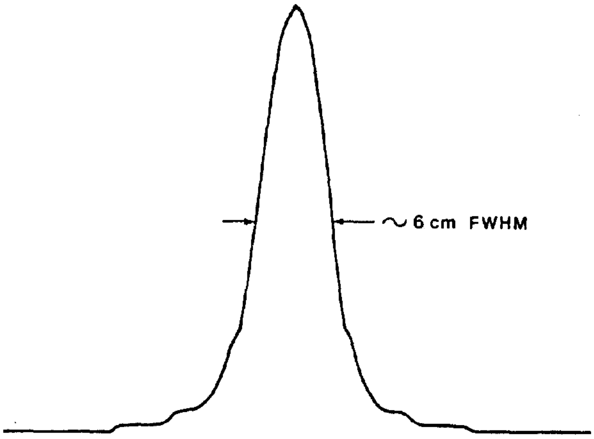

Figure 2. Experimental Distribution of Time of Flight Measurement Errors. Data were obtained by measuring the differential time of flight of annihilation photons emanating from a point source of radioactivity located midway between two opposing scintillation detectors.

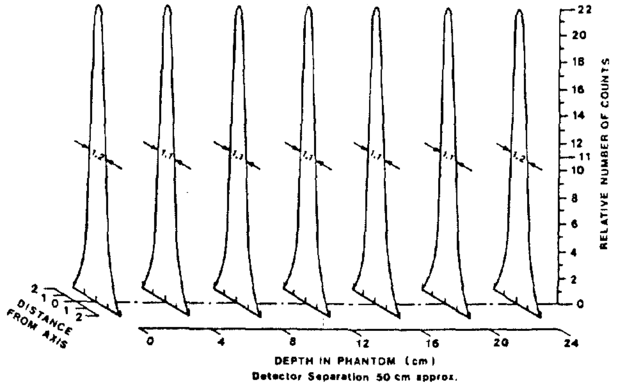

Figure 3. Experimental Distribution of Errors Due to Finite Detector Size. Data were obtained by observing annihilation photons emanating from a point source of radioactivity located at various distances between two opposing detectors. For each distance the source was moved transverse to the line connecting the detectors.

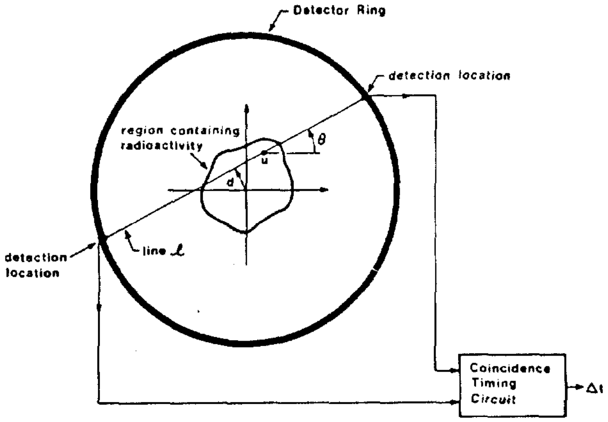

Figure 4. Measurement Point Process Model. Each measurement is a point with coordinates (u,θ).

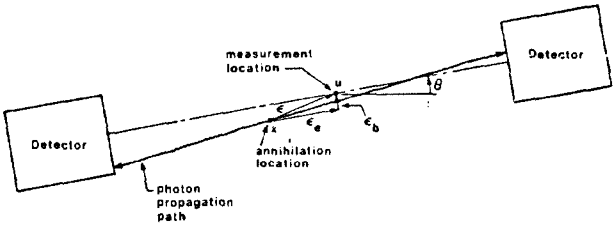

Figure 5. Measurement Point Process Error Model. Each measurement point (u,θ) is a translation of an annihilation point x by an error vector ε(θ).

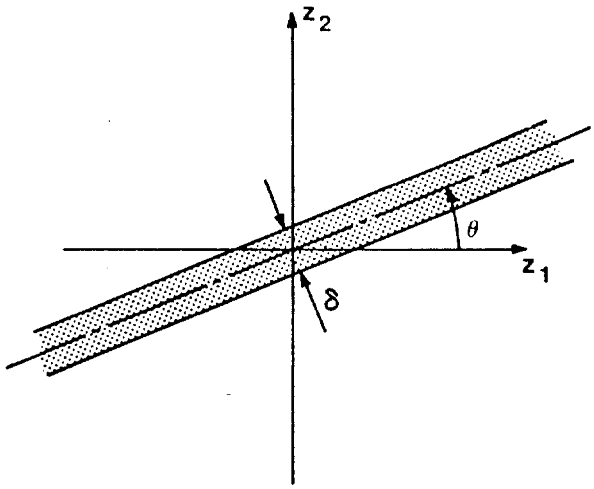

Figure 6. Weighting Function for a Projection Array.

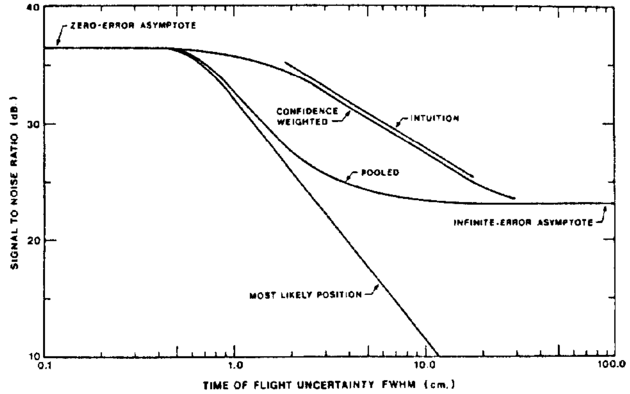

Figure 7. Performance Comparison. Shown are graphs of signal-to-noise ratio as a function of time of flight uncertainty for several pre-image arrays. A uniform circle of radioactivity is assumed with a 15 cm radius, 10^6 total average counts, and a 2 cm circular resolution for the image array.

Donald L. Snyder (S'60-SM'78) received the B.S. degree in electrical engineering from the University of Southern California, Los Angeles, in 1961 and the M.S. and Ph.D. degrees in electrical engineering from the Massachusetts Institute of Technology in 1963 and 1966, respectively.

From 1966 to 1969 he was on the faculty of the Massachusetts Institute of Technology and served as a consultant to the M.I.T. Lincoln Laboratory. Since 1969, he has been on the electrical engineering faculty of Washington University in St. Louis, Missouri. He also served as Associate Director of the Biomedical Computer Laboratory, Washington University School of Medicine. He is presently Chairman of the Department of Electrical Engineering.

Dr. Snyder is the author of papers on the theories of random processes, estimation, decision, and systems and the application of these theories to practical problems arising in communication, control, and biomedical engineering. Most recently, his interest has been in the development and application of random point process models in optical communication and radiology. He is the author of the textbook, *Random Point Processes* (Wiley, 1975), which develops point process models with emphasis on applications.

Dr. Snyder served as Associate Editor for Random Processes for the IEEE Transactions on Information Theory and is the 1981 President of the IEEE Information Theory Group. He is a member of the IEEE Publications Board and is the Program Chairman of the St. Louis chapter of the IEEE Communications Society.

Michel M. Ter-Pogossian, Professor of Radiation Sciences at the Edward Mallinckrodt Institute of Radiology, Washington University School of Medicine, in St. Louis, Missouri, studed as an undergraduate at the Lycée Michlet in Paris and earned his bachelor's degree in mathematics from the University of Paris. While engaged in graduate research in physics at the university, he spent a year at the Institute of Radium studying under Irene Joliot-Curie. He continued his graduate work in nuclear physics at Washington University, receiving his master's and Ph.D. degrees in 1948 and 1950. Dr. Ter-Pogossian's research in positron emission tomography at Washington University School of Medicine has led to the installation of the first American medical cyclotron in the university's Barnard Hospital.

Lewis J. Thomas, Jr., is Director of the Biomedical Computer Laboratory and an Associate Professor of Physiology and Biophysics, and Anesthesiology at the Washington University School of Medicine and Associate Professor of Biomedical Engineering and Electrical Engineering at the Washington University Sever Institute of Technology. He earned his B.S. at Haverford College and his M.D. at Washington University in 1957. Following his residency training at Barnes Hospital, he concentrated on physiologic research in respiration and circulation before joining the Biomedical Computer Laboratory in 1972. He is a member of the American Physiological Society, the American Society of Anesthesiologists, the American Board of Anesthesiology, the New York Academy of Sciences, the American Heart Association, and the American Association for the Advancement of Science.